AIP | Applied Physics Letters

Synthesis and exchange bias effect of single-crystalline $SrMn_3O_{6-\delta}$ nanoribbons

J. Y. Yu, S. L. Tang, X. K. Zhang, L. Zhai, Y. G. Shi et al.

Citation: Appl. Phys. Lett. **94**, 182506 (2009); doi: 10.1063/1.3132056
View online: http://dx.doi.org/10.1063/1.3132056
View Table of Contents: http://apl.aip.org/resource/1/APPLAB/v94/i18
Published by the American Institute of Physics.

Synthesis and exchange bias effect of single-crystalline $SrMn_3O_{6-\delta}$ nanoribbons

J. Y. Yu,[1,2] S. L. Tang,[1,a)] X. K. Zhang,[1] L. Zhai,[1] Y. G. Shi,[1] Y. Deng,[1] and Y. W. Du[1]
[1]*Department of Physics and Nanjing National Laboratory of Microstructures, Nanjing University, Nanjing 210093, People's Republic of China and Jiangsu Provincial Laboratory for NanoTechnology, Nanjing 210093, People's Republic of China*
[2]*Department of Mathematics and Physics, Anhui Institute of Architecture and Industry, Hefei 230022, People's Republic of China*

(Received 27 February 2009; accepted 18 April 2009; published online 7 May 2009)

Single-crystalline $SrMn_3O_{6-\delta}$ nanoribbons (width of 30–500 nm and lengths of up to several hundred micrometers) are synthesized by a molten-salt method. In contrast with the antiferromagnetism in bulk $SrMn_3O_{6-\delta}$, magnetization measurements show weak ferromagnetism in these nanoribbons at low temperature. In particular, a notable exchange-bias effect, which strongly depends on the cooling field, is observed in applied magnetic field $H \leq 5$ kOe. These results suggest that the exchange bias in the $SrMn_3O_{6-\delta}$ nanoribbons can be effectively tuned by the cooling field, which is of very special interests for applications. © *2009 American Institute of Physics*. [DOI: 10.1063/1.3132056]

One-dimensional (1D) nanostructures such as nanotubes, nanoribbons, and nanowires are not only of scientific but also technological interests. The inherent anisotropy in these nanomaterials provides unique properties which are expected to be critical to the function and integration of nanoscale devices.[1–3] Among these materials, 1D nanostructural manganites have been of particular interests for magnetic sensing and recording devices, as they exhibit unique magnetoelectric properties.[4–7] Investigations have shown that these properties are critically dependent on the dimensions of the material.[5–7] Although advances have been made in the fabrication of nano- and microcrystalline manganites,[8,9] detailed physical investigations of 1D nanocrystalline manganites have not been possible due to the lack of reliable methods to prepare well-isolated manganite 1D nanostructures with various stoichiometry or crystal structures.

Here, we report a simple molten-salt method to prepare the nominal $SrMn_3O_{6-\delta}$ nanoribbons. The structure of $SrMn_3O_{6-\delta}$ consists of unusual "figure-of-eight" shaped tunnels. These tunnels are made up of double chains of edge- and corner-sharing MnO_6 octahedra, with the Sr^{2+} ions situated in the tunnel cavities, which is a complex incommensurate modulated tunnel structure.[10,11] In the well-known double chains of MnO_6 octahedra systems, quantum spin fluctuations or geometric frustration play a very important role, which can lead to various magnetic ground state such as antiferromagnetic (AFM) order, ferromagnetic (FM) order, spin-glass (SG) order, and complex multistate coexistence.[12] In particular, the exchange bias caused by the exchange interaction at the interface between a FM and an AFM component draws a significant interest in recent years.[13,14] In general, the exchange bias is manifested by a shift in the hysteresis loop along the field axis, when the FM-AFM system is cooled down in an external magnetic field through the Néel temperature of the antiferromagnet. But recent studies have shown that, in addition to FM/AFM systems, exchange bias phenomenon was also observed in samples involving a ferrimagnet (FI) or a SG phase (FI/AFM, FM/SG, SG/AFM).[15] In this article, the single crystalline $SrMn_3O_{6-\delta}$ nanoribbons show an appearance of weak ferromagnetism and exchange bias effect at low temperature, which is distinct from their bulk counterparts with a typical AFM order ($T_N \sim 46$ K).[10]

Single crystalline $SrMn_3O_{6-\delta}$ nanoribbons were prepared by a molten-salt method. Polycrystalline $SrMnO_3$ powders (purity: 99.9%) and chlorides (molar ratio NaCl/KCl=1:1) at a weight ratio of 2% were thoroughly mixed in an agate pestle and mortar before being transferred into an alumina crucible. The source materials were heated to 800 °C at a heating rate of 5 °C/min for 5 h and then cooled naturally to room temperature. The resulting powders were collected and washed with distilled water. The crystallization and morphology of the $SrMn_3O_{6-\delta}$ nanoribbons were investigated by x-ray diffraction (XRD), scanning electron microscope (SEM), and transmission electron microscope (TEM). As a function of T and H, the magnetization (M) was measured using superconducting quantum interference device magnetometer.

Low magnification SEM observations shown in Fig. 1(a) reveal that the as-synthesized products consist of a large quantity of 1D nanostructures with typical lengths from tens to hundreds micrometers. Energy dispersive x-ray spectroscopy (EDS) microanalysis as the inset in Fig. 1(a) shows the presence of the elements O, Sr, and Mn. The EDS analysis revealing that the molar ratio of Sr:Mn:O is about 1.00:3.05:5.95 within the instrumental accuracy. The XRD pattern in Fig. 1(b) shows that the as-synthesized product is orthorhombic $SrMn_3O_{6-\delta}$ (Ref. 16) with lattice constants of a=9.133 Å, b=2.821 Å, and c=12.095 Å.[10] The TEM images of $SrMn_3O_{6-\delta}$ are shown in Figs. 2(a) and 2(b). Selected area electron diffraction (SAED) patterns of a single nanoribbon, as shown in the inset of Fig. 2(a), indicates that the nanoribbon is a single crystal, which is further proved by high-resolution TEM image [inset in Fig. 2(a)]. The TEM images in Fig. 2(b) reveal that each $SrMn_3O_{6-\delta}$ nanoribbon

a)Author to whom correspondence should be addressed. Electronic mail: tangsl@nju.edu.cn.

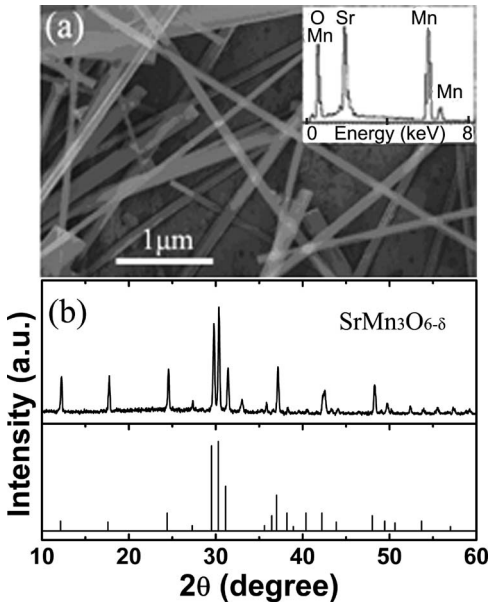

FIG. 1. (a) SEM image of the as-synthesized $SrMn_3O_{6-\delta}$ nanoribbons and their EDS pattern (inset a). (b) XRD pattern of the nanoribbons. The JCPDS Card No. 28–1233 database standard ($SrMn_3O_{6-\delta}$) is shown at the lower part of panel b.

has a uniform width within 20–200 nm. To further verify the morphological characteristic of the nanoribbons, a cross-sectional TEM image of rectanglelike-shaped end of a ribbon around 40 nm thick is given in Fig. 2(b) inset.

To explore the original magnetic phase in $SrMn_3O_{6-\delta}$ nanoribbons, we carried out magnetic measurements. Figure 3 shows the temperature dependent magnetization $M(T)$ curves of the nanoribbons in zero-field-cooled (ZFC) and field-cooled (FC) processes with an applied field of 2 kOe. The ZFC magnetization curve exhibits a sharp peak at $T_m(\sim 26\ \mathrm{K})$ accompanied by a clear bifurcation of ZFC and FC magnetization curves, which indicates a glassy behavior at low temperature.[9,17] Simultaneously, the linear fit for the temperature dependence of the inverse magnetization shows that the material exhibits Curie–Weiss behavior above about 50 K and gives an extrapolated Curie–Weiss temperature (θ) of 150 K higher than the one of bulk ($\theta \approx -450\ \mathrm{K}$),[10] which indicates that the AFM phase is weakened in the nanosized $SrMn_3O_{6-\delta}$. In particular, an anomalous behavior is seen below ~10 K, i.e., both curves (FC and ZFC) show sudden increase in magnetization, pointing out the weak FM tendency at low temperature. It has been reported that oxygen

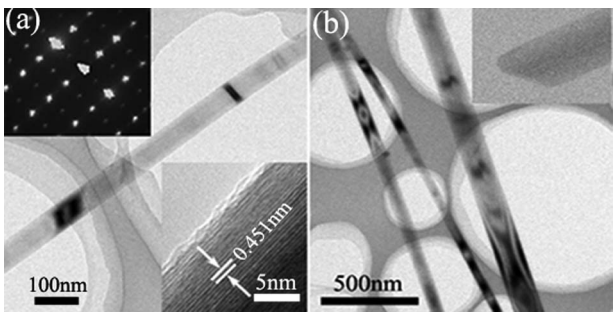

FIG. 2. (a) Typical TEM micrograph of $SrMn_3O_{6-\delta}$ nanoribbon. Insets are the corresponding SAED pattern (upper left) and high-resolution TEM image (lower right). (b) TEM images of several straight nanoribbons. Inset is a rectanglelike-shaped end of a nanoribbon.

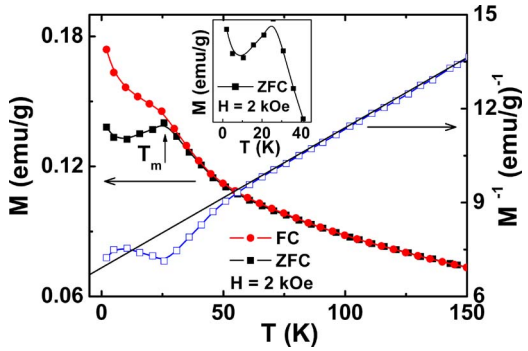

FIG. 3. (Color online) Temperature dependence of the magnetization $M(T)$ of $SrMn_3O_{6-\delta}$ nanoribbons for ZFC and FC under a 2 kOe field (left axis) and inverse magnetization versus temperature (right axis). Solid line represents linear fit between 50 and 150 K. Inset: enlargement of $M \sim T$ curve under ZFC below 40 K.

vacancies can also lead to an anomalous magnetic behavior in manganites. For example, $CaMnO_{3-\delta}$ nanoparticles[18] and $La_xCa_{1-x}MnO_{3-\delta}$ single crystals[19] show a weak FM phase due to formation of FM clusters near defects. Recently, studies have shown that the antiferromagnetism in bulk manganites is suppressed in both nanowires and nanoparticles, accompanied with an appearance of weak ferromagnetism.[6,20] A core-shell phenomenological model was proposed, where the relaxation of superexchange interaction on the surface of nanowires or nanoparticles allows the formation of a FM or SG shell, resulting in natural AFM/FM or FM/SG interface.[18,21] Considering the SG-like characteristic of magnetization curves in Fig. 3 and the unsaturated M-H curve at 3 K in fields up to 5 kOe like other conventional SG systems in Fig. 4, a similar description, an AFM core and a SG-like

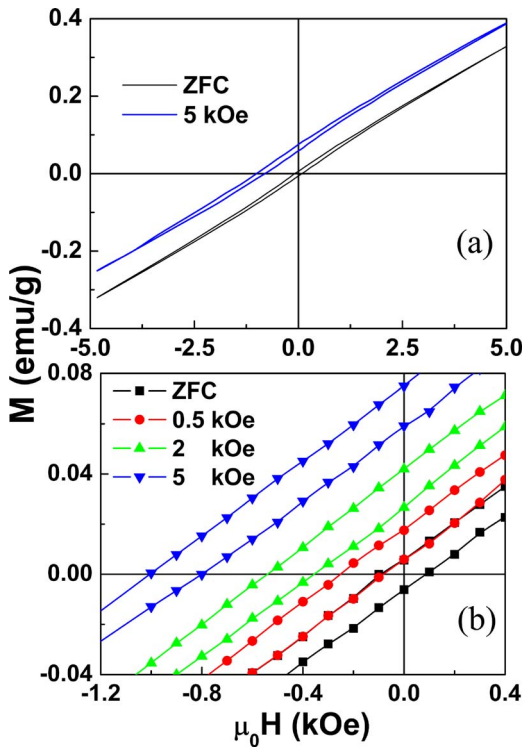

FIG. 4. (Color online) (a) Magnetization as a function of external magnetic field at 3 K for $SrMn_3O_{6-\delta}$ nanoribbons. (b) Shows the enlarged view of the low field region, which indicates the shift of the hysteresis curve due to exchange bias coupling.

shell, for the magnetic structure of the $SrMn_3O_{6-\delta}$ nanoribbons could be easily guessed, where the SG-like surface layers may act as the weak "FM" on AFM nanoribbons.[15] The SG-like order probably arises as a result of the higher surface-to-volume ratio afforded by the nanoribbon geometry, i.e., surface effects, which can result in uncompensated spin and a suppression of the long-range AFM order observed in the bulk. The clarification as to whether any or all of these factors are operative behind our observation is beyond the scope of this present work and will form the subject of future studies.

As mentioned above, exchange bias is manifested as the hysteresis loop shift observed when an antiferromagnet is in contact with a ferromagnet or SG.[15] Thus, exchange bias could also be expected based on the fact that there exists a coupling between the SG-like shell and the AFM core in the $SrMn_3O_{6-\delta}$ nanoribbons. To prove it, we measured the hysteresis loops of the nanoribbons at 3 K after both the ZFC and the FC processes from 300 K under a magnetic field of 5 kOe, as shown in Fig. 4. It is also observed in the hysteresis curve that the saturation did not show in fields up to 5 kOe like other conventional SG systems.[17] The observed *M-H* curve at 3 K reveals weak ferromagnetism probably due to spin freezing. The ZFC hysteresis loop keeps good central symmetry with a coercive field of $H_C \sim 95$ Oe. However, for the FC process, where the sample was cooled in magnetic field of 0.5, 2, and 5 kOe respectively from 300 to 3 K, asymmetrical magnetic hysteresis loop exhibiting shifts both in the field and magnetization axes is observed, which reveals the existence of exchange coupling in the nanoribbons. We notice that traces of hysteresis are closed loops for $H_{max} \geq 3$ kOe shown in Fig. 4(a), where H_{max} is the maximum field applied for the loop trace. Therefore, hysteresis loop with $H_{max}=5$ kOe in Fig. 4 is not a minor loop, indicating the exchange bias effect in $SrMn_3O_{6-\delta}$ nanoribbons is a genuine observation which is not a simplified phenomenon of the minor loop effect of a ferromagnet.[22] We define the exchange bias field as $H_E=-(H_1+H_2)/2$, where H_1 and H_2 are the left and right coercive fields, respectively. For the FC loops in magnetic field of 0.5, 2, and 5 kOe, the value of H_E is about 165, 450, and 860 Oe, respectively, indicating the exchange bias is strongly dependent on the cooling field. The shift to positive magnetization axis for the FC loops suggests the presence of a unidirectional exchange anisotropy interaction.[15] The remanence asymmetry M_E, defined as the vertical axis equivalent to H_E, is about 0.012 emu/g for the FC loop of 0.5 kOe and 0.065 emu/g for the one of 5 kOe respectively. Results indicate that the exchange bias in the $SrMn_3O_{6-\delta}$ nanoribbons increase with the increasing cooling field. It could be explained simply, for small cooling fields, only a part of spins at the SG/AFM interface are pinned along the cooling field direction. With the increase in the cooling field, more of the spins are pinned along the field direction and the exchange interaction is enhanced. Accordingly, H_E increases with the cooling field. It means that the exchange bias in the nanoribbons can be tuned by the cooling field, which contributes to the development of multifunctional spintronic devices.

In summary, we have developed a facile molten-salt synthesis method to prepare long single-crystalline $SrMn_3O_{6-\delta}$ nanoribbons and characterized them by various techniques. Magnetization measurements show that these nanoribbons exhibit weak ferromagnetism at low temperature. A significant exchange bias phenomenon, which is strongly dependent on the cooling field, is observed in the 1D $SrMn_3O_{6-\delta}$ system. Our results suggest that the exchange bias in the 1D manganite can be effectively tuned by the cooling field, which is of very special interests for applications.

This work was supported by the National Key Project of Fundamental Research of China (Grant No. 2005CB623605).

[1] G. R. Patzke, F. Krumeich, and R. Nesper, Angew. Chem., Int. Ed. **41**, 2446 (2002).
[2] Z. Y. Tang and N. A. Kotov, Adv. Mater. (Weinheim, Ger.) **17**, 951 (2005).
[3] T. Shimada, S. Tomoda, and T. Kitamura, Phys. Rev. B **79**, 024102 (2009).
[4] N. Wang, C. G. Hu, C. H. Xia, B. Feng, Z. W. Zhang, Y. Xi, and Y. F. Xiong, Appl. Phys. Lett. **90**, 163111 (2007).
[5] K. S. Shankar, S. Kar, and A. K. Raychaudhuri, Appl. Phys. Lett. **84**, 993 (2004).
[6] S. S. Rao, S. Tripathi, D. Pandey, and S. V. Bhat, Phys. Rev. B **74**, 144416 (2006).
[7] D. C. Arnold, O. Kazakova, G. Audoit, J. M. Tobin, J. S. Kulkarni, S. Nikitenko, M. A. Morris, and J. D. Holmes, ChemPhysChem **8**, 1694 (2007).
[8] J. J. Urban, L. Ouyang, M. H. Jo, D. S. Wang, and H. Park, Nano Lett. **4**, 1547 (2004).
[9] S. M. Zhou, L. Shi, H. P. Yang, Y. Wang, L. F. He, and J. Y. Zhao, Appl. Phys. Lett. **93**, 182509 (2008).
[10] L. J. Gillie, J. Hadermann, O. Pérez, C. Martin, M. Hervieu, and E. Suard, J. Solid State Chem. **177**, 3383 (2004).
[11] A. N. Grundy, B. Hallstedt, and L. J. Gauckler, J. Phase Equilib. Diffus. **25**, 311 (2004).
[12] C. H. Booth, F. Bridges, G. H. Kwei, J. M. Lawrence, A. L. Cornelius, and J. J. Neumeier, Phys. Rev. Lett. **80**, 853 (1998).
[13] D. Niebieskikwiat and M. B. Salamon, Phys. Rev. B **72**, 174422 (2005).
[14] T. Qian, G. Li, T. F. Zhou, X. Q. Xiang, X. W. Kang, and X. G. Li, Appl. Phys. Lett. **90**, 012503 (2007).
[15] J. Nogués, J. Sort, V. Langlais, V. Skumryev, S. Suriñach, J. S. Muñoz, and M. D. Baró, Phys. Rep. **422**, 65 (2005).
[16] JCPDS Card No. 28–1233.
[17] S. Karmakar, S. Taran, E. Bose, and B. K. Chaudhuri, Phys. Rev. B **77**, 144409 (2008).
[18] V. Markovich, I. Fita, A. Wisniewski, R. Puzniak, D. Mogilyansky, L. Titelman, L. Vradman, M. Herskowitz, and G. Gorodetsky, Phys. Rev. B **77**, 054410 (2008).
[19] N. N. Loshkareva, A. V. Korolev, T. I. Arbuzova, N. I. Solin, A. M. Balbashov, and N. V. Kostromitina, Phys. Met. Metallogr. **103**, 251 (2007).
[20] D. L. Zhu, H. Zhu, and Y. H. Zhang, Appl. Phys. Lett. **80**, 1634 (2002).
[21] S. Dong, F. Gao, Z. Q. Wang, J.-M. Liu, and Z. F. Ren, Appl. Phys. Lett. **90**, 082508 (2007).
[22] M. Patra, M. Thakur, K. De, S. Majumdar, and S. Giri, J. Phys.: Condens. Matter **21**, 078002 (2009).